Wrinkling Suppression in Thin Membranes using Designed Geometrical Features

Mohammad Nazzal*[a,b], Maen Alkhader[a], Akshat Agha[c], Fadi Abu-Farha[c], Zain Ali[a], Waleed AlDamaty[a]

[a] Department of Mechanical Engineering, American University of Sharjah, Sharjah, UAE
[b] Department of Mechanical Engineering, German Jordanian University, Madaba, Jordan
[c] Clemson University-International Centre for Automotive Research (CU-ICAR), 4 Research Drive, Greenville, SC 29607, United States
*Corresponding Author, email: mnazzal@aus.edu

Abstract

The rapidly increasing use of thin membranes; especially in the fabrication of flexible electronics, has motivated investigating the wrinkling behavior of these membranes. Wrinkling has an undesirable effect since wrinkles degrade the surface accuracy of structures incorporating thin membranes. This work introduces and evaluates an approach based on including optimized geometric features in thin membranes to suppress their wrinkling behavior. The ability of the optimized geometric features to suppress wrinkling in a 25 μm thick polyimide membrane subjected to uniaxial stretching is investigated computationally and experimentally in this work. A finite element model is developed to predict the wrinkling behavior of the membrane. An experimental setup equipped with 3D digital image correlation system is used to determine the wrinkles pattern, amplitude, and wavelength. Symmetric circular holes are introduced in the membrane to redistribute the stress field, eliminate the fluctuation in the minor principal stress in the membrane, and suppress wrinkles. The location and size of the circular holes are determined by coupling the Non Linear Programming by Quadratic Largrangian technique and finite element simulations. An optimal design is obtained and the experimental results show that the optimally designed holes effectively suppressed the wrinkling behavior.

Keywords

Thin membranes; post buckling analysis; wrinkling suppression; full field digital image correlation, optimization

1. Introduction

Factors such as flexibility, ultralight weight, ease of stowage and folding in a low packaging volume have given thin membranes in general and Kapton® HN polyimide thin films in particular rapid popularity in electronics, aerospace, and civil construction industries. In the electronics industry, thin membranes are used as supporting flexible substrates in the fabrication of new generation flexible electronics. For instance, Mamleyev et al [1] used optimized laser radiation to pattern graphitic carbon structures onto Kapton® films for the fabrication of flexible devices. Romero et al [2] used inkjet-printing to fabricate planar interdigitated electrode capacitors with Kapton® film as supporting flexible substrate. Zhang et al [3] fabricated a flexible rectenna for Wi-Fi-band wireless energy harvesting on a Kapton® film. In the aerospace industry, thin membranes such as Kapton® are heavily used in space based gossamer structures [4]. Gossamer structures are packaged in a very small volume and deployed in space by spinning, inflation or other means. The use of such structures significantly reduce the space mission cost by reducing the launch vehicle size requirement. Recently, NASA [5, 6] developed and tested a large inflatable solar array that consists of thin film solar cells mounted on a Kapton® film. The inflatable solar array is significantly lighter in weight, easier to package and deploy, and can harnesses more energy when compared to the rigid deployable solar arrays. Other applications using thin films include solar sails, thermal insulation on electrical traction motors, sensor mats, and radar antennas.

A main characteristic of thin membranes is their poor handling of compressive loads; in particular, they have high propensity to buckle when subjected to compressive loads. Accordingly, applications involving thin membranes are designed to comprise mainly tensile loadings. Yet, under tensile loading membranes often tend to develop wrinkles. Wrinkles in thin membranes are out of plane buckling-based deformations. They develop due to the negligible flexural stiffness of thin membranes, and they are triggered by the induced compressive stress along the minor principal stress direction (e.g., the direction perpendicular to the loading direction in case of uniaxial loading).

The two most common approaches used in literature to analyze wrinkling in elastic membranes are the tension field theory [7-12] and the bifurcation analysis [13-15]. The tension field theory approach was first proposed by Wagner [7] to estimate shear loads in flat sheet metal girders with very thin metal web. Wagner assumed that the membrane has zero bending stiffness. Based on this theory, Stein and Hedgepeth [8] predicted stresses and deformations of stretched membranes for loads at which the membranes wrinkle. Ding and Yang [9] further extended Stein's model by changing the Young's modulus along with the Poisson's ratio to study their effects on wrinkling behavior. Coman [10] investigated the wrinkling instability of a pre-stressed annular membrane loaded uniformly along its inner boundary using the tension field theory. Coman [10] concluded that the theoretical solution can capture the essential qualitative features involved in axisymmetric wrinkling. However, the theoretical solution displays several limitations regarding the quantitative aspects of wrinkling such as amplitude, wavelength, and number of wrinkles. This is a main shortcoming of the tension field theory. On the other hand, the critical conditions for wrinkling and post buckling behavior can be predicted using the

bifurcation analysis approach. In this approach, the membrane is treated as a thin shell with non-zero bending stiffness. A typical wrinkling analysis based on the bifurcation analysis consists of three steps. In the first step, the membrane is pre-stressed. In the second step, an eigenvalue buckling analysis is performed to obtain the critical buckling loads and the buckling modes. In the third step, the mode shapes determined in the previous step are superimposed on the membrane as geometrical imperfections and a post buckling analysis is conducted. This approach is often applied using computational methods such as Finite Element (FE) analysis to elucidate the wrinkling behavior of membranes. For instance, Nayyar et al [14], using bifurcation theory and FE analysis, studied stretch-induced wrinkling of hyperelastic rectangular sheets under uniaxial stretching. Their results showed that the critical condition for wrinkling and the post-buckling behavior depend on the sheet thickness. Lecieux and Bouzidi [15] experimentally and computationally, using finite element analysis and bifurcation theory, analyzed the formation and evolution of wrinkle patterns in cruciform membrane specimens. Their post-buckling FE analysis results in terms of shape, amplitude, and wavelength of the wrinkles agreed well with experiments. Due to its robustness and ability to predict post buckling behavior, the bifurcation analysis approach has been the method of choice in several recent efforts focused on elucidating wrinkling behavior of thin membranes [16-19].

Wrinkling has an undesirable effect in many applications as it might undermine the capability and performance of structures. An example to realize the seriousness of this undesired effect could be that of a membrane reflector. Curvatures introduced by wrinkling would cause a curved reflecting surface or a non-uniform surface heating in solar sails. Several researchers tackled the issue of wrinkling, wrinkling suppression and tuning using different techniques [20-26].

Zheng [20] examined wrinkling suppression of dielectric elastomeric membranes using electric field-induced actuation. The membrane was coated on each side with a compliant electrode. Electric field was applied to the wrinkled membrane and the dynamic structural response of the membrane was captured experimentally. A significant decrease in the wrinkling amplitude was observed due to the electric field-induced actuation. Li et al [21] proposed wrinkle free graphene membranes by adopting optimal designs obtained through topology optimization. Luo et al [22] considered a wrinkle free design of thin Kapton membrane using topology optimization. The objective of topology optimization in their work is to find the stiffest design that satisfies the principal stress constraints for wrinkling avoidance and the area constraints in order to sustain the performance requirements. Li et al[27] developed a new technique for wrinkling suppression by applying an optimally distributed spatioselective coating layer that is determined based on non-gradient topology optimization algorithm. It is noteworthy to mention that topology optimization of membranes without adding new coating layers has an adverse effect on the surface area as the optimal designs might suffer from area loss that results from topology optimization. On the hand, coating layers add new material to the membrane that might affect its functionality. Another approach for tailoring the elastic deformation patterns of elastomers is by designing special microstructures [28, 29]. Bertoldi et al [28] created an auxetic honeycomb structure by introducing a square lattice of circular holes in a silicone rubber cellular solid. Yan et al [29] proposed a method to tailor wrinkling patterns of membranes by introducing simple microstructures presented as holes to redistribute the stress field. Several wrinkle patterns were demonstrated by varying the holes patterns.

The aforementioned approaches for wrinkling suppression and control showed that topology optimization, though it has shortcomings, can effectively suppress wrinkling, and introducing microstructures in thin membranes can control their wrinkling patterns. This work draws on these findings and integrates them to develop a new approach for wrinkling suppression in thin membranes during elastic deformation. In the new approach, geometrical features that consist of holes are introduced to redistribute the stress field in thin membranes and minimize their out of plane deformation (wrinkling). Moreover, the size and location of the introduced holes that result in changing the stress distribution, minimize induced compressive stresses, and effectively suppress wrinkling are determined using FE analysis and the Non Linear Programming by Quadratic Largrangian (NLPQL) technique. Thus, in summary, in the new approach wrinkling is suppressed through the introduction of holes of specific sizes at specified locations. Experiments using three-dimensional Digital Image Correlation (3D DIC) are used to verify the effectiveness of the new approach in suppressing wrinkling.

2. Methods

2.1 Material and Experimental Setup

A rectangular membrane that has two clamped ends subjected to uniaxial tensile load is analyzed to demonstrate the effectiveness of the proposed wrinkling suppression approach. The dimensions of the membrane are selected following the critical aspect ratios defined by Zheng [20] for thin membranes with large surface area. Zheng [20] showed that membranes with large surface area relative to their thickness and intermediate aspect ratios (i.e., Length to width ratio) around 2 have lower structural stability and high propensity for wrinkling. Accordingly, the membrane of Figure 1 is selected to have an aspect ratio of 2 (L= 100 mm, W= 50 mm) and a small thickness of

25 µm. These dimensions allow for evaluating the effectiveness of the new approach in suppressing wrinkling in a challenging problem (i.e., has very high propensity for wrinkling).

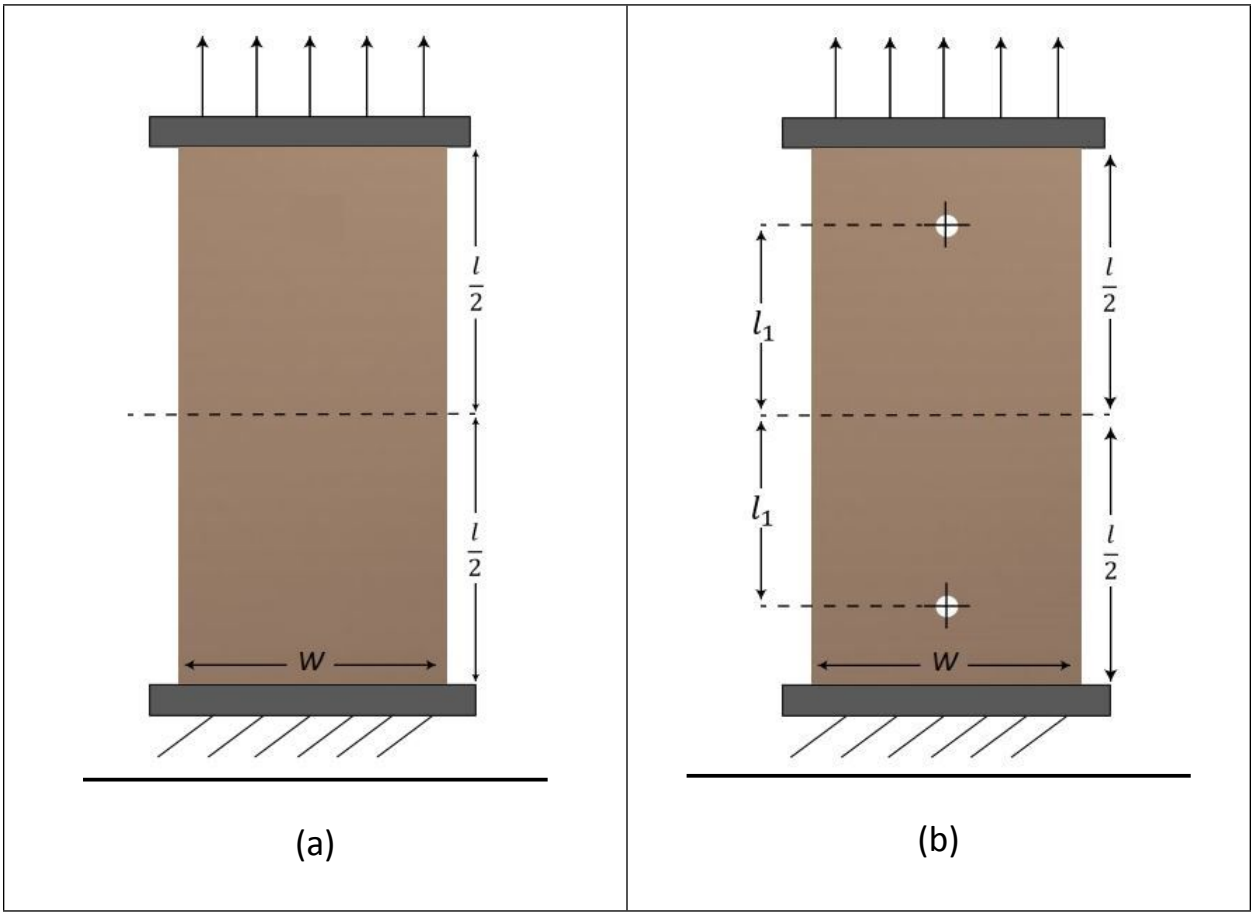

Figure 1. Schematic of the rectangular membrane under investigation. (a) original membrane (b) membrane with geometrical modification. (*L=100 mm, W=50 mm*)

The membrane considered in this work is made of a commercial DuPont™ Kapton® HN polyimide film with a thickness of 25 µm, modulus of elasticity of 2.5 GPa, Poisson's ratio of 0.34 and yield strain of 4% [30]. This material has been used successfully in applications at temperatures as low as -269°C and as high as 400°C [30]. It can be laminated, metallized, punched, formed or adhesive coated. Membrane specimens were cut into rectangular shapes of 150 mm length and 50 mm width. Masking tape was applied at the gripped regions of the specimen to provide rigidity to the gripping area in order to ensure zero slippage. The unmasked region has an aspect ratio of

2 (L= 100 mm, W= 50 mm). Few of the cut specimens were modified geometrically by including holes in them as shown schematically in Figure 1 (b). The exact size and location of the holes are discussed in the optimization section in this work. Thus, two sets of specimens were prepared, with and without holes. Both sets were subjected to the same experimental procedure to investigate their propensity for wrinkling under uniaxial stretching.

Kapton® membrane specimens were subjected to uniaxial stretching tests. These were performed on a 5985 INSTRON electromechanical load frame with a 500 N load cell. Special grips suitable for testing thin membranes were used to prevent specimen slippage. All tensile tests were conducted at room temperature and cross head velocity of 0.25 mm/s. Figure 2 shows the experimental setup that consists of the Instron loading frame, specimen with speckle pattern applied to it, load cell used to measure the loading force, and the ARAMIS 3D Digital Image Correlation (3D-DIC) system. A full field multi-camera 3D DIC system is used in this work to capture the out of plane deformation and the wrinkling behavior of the tested membranes. Two 5 Megapixel CCD cameras were used in combination with lenses that offer manual control of focus, zoom, and aperture. Optimum object illumination is obtained through two high-performance dual LEDs. The typical resolution in displacement for this system is less than 0.1 pixel; which is equivalent to $8\ \mu m$ considering the target area (field of view) of our specimen. A random speckle pattern was created by painting the surface of the specimen as shown in the zoomed-in window in Figure 2. This pattern generates the contrast needed for the DIC system. Digital images were recorded at the rate of 5 frames per second during experiments and were post-processed to obtain X, Y, Z displacement history of each point in the unmasked region throughout the test.

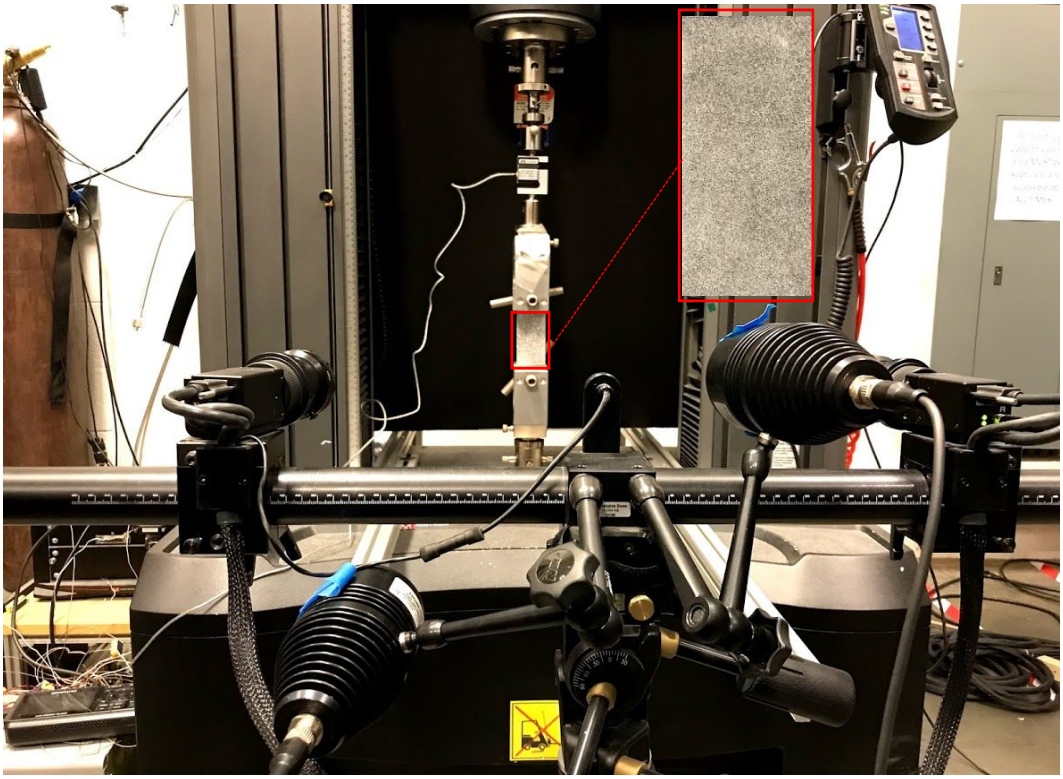

Figure 2. Experimental Setup with the 3D optical strain field measurement system.

2.2 Finite Element Analysis of Wrinkling Behavior

In this section, the FE model and FE analysis procedure used to model wrinkling of thin membranes are presented. FE analysis is performed using ABAQUS 2017. The FE procedure presented here is used to model wrinkling in specimens with and without geometric modifications (i.e., holes). However, the procedure is illustrated here through applying it to the case of specimens without geometric modification. FE models mimicking the experimentally tested membrane specimens are developed first. The FE model of the uniaxially stretched membrane specimens without any geometric modification is shown in Figure 3. The model has the dimension of 100mmx50mm. The elastic properties mentioned in the previous section were

used to define the material behavior in the FE model. Yan et al[29] captured the wrinkling behavior of the same material successfully using a linear elastic model. The linear elastic model is favored in this work due to its ability to capture the wrinkling behavior at low computational cost. The membrane is modeled using the quadrilateral general-purpose reduced integration shell elements (S4R) that are based on first-order shear deformation theory. These elements are capable of handling finite membrane strains and arbitrary large rotations. The FE analysis procedure used in this work to predict and analyze the wrinkling behavior of thin membranes follows the finite element based bifurcation analysis approach used by Zheng [20] as well as Lecieux and Bouzidi [15]. The FE procedure consists of the following three steps, which are schematically shown in Figure 4:

- In the first step, a small uniaxial edge displacement is applied to the membrane edge to pre-stress the membrane and obtain an initial stable state (base state). Applied displacement acts as the tensile preload that provides initial geometric stiffness prior to the buckling analysis. The value of the applied edge displacement is determined through an iterative process. The displacement corresponding to the smallest preload that results in positive eigenvalues in the linear perturbation buckling analysis is sought and applied to the model. The pre-load displacement is applied to the nodes lying on the membrane's top edge, along their vertical direction. Moreover, to mimic the loading conditions shown in Figure 2, the vertical and horizontal displacements of the nodes on the membrane's bottom edge are fixed, and the horizontal displacements of the nodes at the top edge of the membrane are fixed. This step uses the nonlinear static solver in ABAQUS which

accounts for geometric nonlinearities. At the end of this step, equilibrium under the applied pre-load is achieved, and the pre-stresses in the membrane are determined.

- In the second step, a linear perturbation buckling analysis is performed using ABAQUS to extract the eigenvalues and determine the critical buckling modes. In this step and according to ABAQUS's theory and implementation manuals [31], an incremental perturbation load Q^N in the form of edge displacement is introduced and scaled by the load multipliers λ_i. With the incremental load, the equilibrium equation governing the behavior of the membrane takes the form of the following eigenvalue problem [31]:

$$(K_0^{MN} + \lambda_i K_\Delta^{MN}) v_i^M = 0 \quad (1)$$

Where K_0^{MN} is the stiffness matrix that corresponds to the base state, and K_Δ^{MN} is the differential initial stress and the load stiffness matrix due to the incremental perturbation load Q^N.The degrees of freedom for the entire model are denoted by M and N. λ_i refers to the eigenvalue and v_i refers to the eigenvector (buckling mode shape) of the ith buckling mode. Note that the magnitude of the incremental perturbation load Q^N is insignificant as it is scaled by the load multiplier. The strain in the membrane, which is referred to as the critical strain (ε_{crit}) since buckling is present, corresponding to the ith buckling mode can be calculated as follows

$$\varepsilon_{crit} = \varepsilon_{pre} + \lambda_i \varepsilon_o \quad (2)$$

where ε_{pre} and ε_o are the pre-strain applied in the first step and the incremental strain applied in the second step by displacing the membrane edge; respectively.

- In the third step, post buckling analysis is carried out. The buckling mode shape that resembles the wrinkling pattern observed in experiments is introduced in the initial

perfect flat membrane before the post buckling response is performed. It is introduced in the membrane structure as geometric imperfections. The magnitude of imperfection is represented as [31]:

$$\Delta x_i = \emptyset_i v_i \quad (3)$$

where $\emptyset_i$ is a scaling factor whose magnitude is a proportion of the membrane thickness and v_i is the ith eigenvector. In a study on wrinkling in Kapton membranes, R. Carvalho [32] has shown that the wrinkles amplitude is independent of the magnitude of the geometric imperfection. Therefore, a scaling factor value of 10% of the membrane thickness is used in all simulations. The post buckling analysis consists mainly of two analysis sub-steps. In the first sub-step, the membrane is pre-tensioned by slightly displacing one edge of the membrane in order to provide initial out of plane stiffness without affecting the final results. Then a geometrically nonlinear incremental analysis under prescribed edge displacement similar to the experimental displacement is performed using the Newton Raphson solution method to simulate post buckling. Pseudo viscous damping forces are introduced at all nodes when instability is detected and dynamic integration of the equations of motion is implemented to simulate the dynamic response of the structure.

http://mc.manuscriptcentral.com/(site)

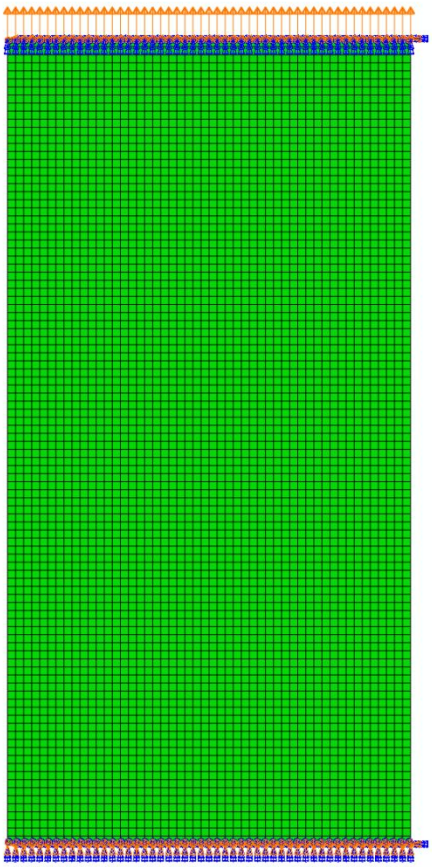

Figure 3. Meshed rectangular membrane with boundary conditions.

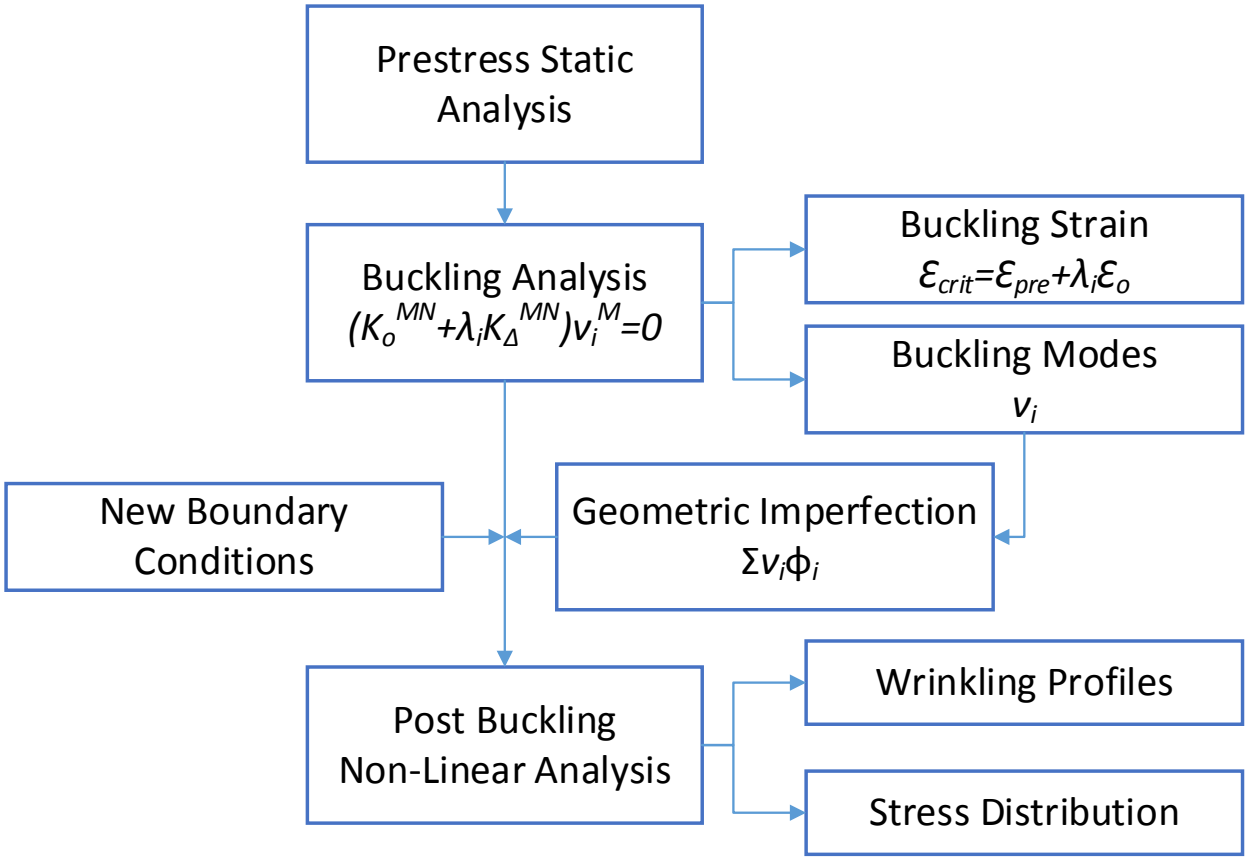

Figure 4. Flow chart for wrinkling analysis simulation

3. Results and Discussion

3.1 Wrinkling analysis of the membrane without geometrical modification

The FE procedure presented in the previous section is applied on the rectangular membrane shown in Figure 3 to extract its eigenmodes and predict its wrinkling behavior under uniaxial stretching. A mesh convergence study based on the lowest eigenvalue and amplitude of wrinkles is carried out first. The results of this study are listed in Table 1. It is found that the FE solution becomes mesh independent when the number of elements exceeds 5000. Therefore, 5000 elements are used in the FE simulations.

Following the presented FE procedure, the preload step is applied first. Accordingly, an edge displacement of 0.6 mm is applied to preload the membrane. This displacement magnitude is found to be the smallest displacement that yields positive eigenvalues.

In the second step of the FE analysis, eigenvalue buckling analysis, an incremental load in the form of an axial edge displacement of 1 mm is applied at the moving edge of the membrane. The first two buckling mode shapes obtained from the FE simulations are shown in Figure 5. The buckling mode shapes are normalized vectors that do not represent the actual magnitudes of deformation at critical loads. They are normalized to ensure that the magnitude of the maximum displacement component has a value of 1. It is observed from Figure 5 that the first two buckling modes occur in pairs, the first one is antisymmetric and the second one is symmetric. Both modes correspond to the lowest eigenvalue that is equal to $\lambda = 0.457$. This indicates that the membrane has numerically an equal chance to deform into either mode beyond the critical buckling strain. Based on this eigenvalue, the critical strain obtained from Equation 2 is $\varepsilon_{crit} = 1.2\%$. The symmetric buckling mode is introduced into the model as geometric imperfection in the membrane before the post buckling analysis is conducted. This mode is chosen because experiments show that the wrinkling pattern is symmetric.

In the post buckling analysis, the membrane is pre-tensioned by displacing the edge of the membrane by 0.1 mm in order to provide initial out of plane stiffness without affecting the final results. Then a geometrically nonlinear incremental analysis with a prescribed edge displacement of 4 mm that corresponds to a 4% tensile strain is performed to simulate the post buckling behavior. A maximum strain value of 4% is chosen here because this investigation is concerned with wrinkling suppression during elastic deformation. Figure 6 shows the wrinkling

http://mc.manuscriptcentral.com/(site)

profiles obtained from FE analysis at the transverse mid-plane at different strains (2%, 3%, 4%). It is observed form this figure that at each strain level five wrinkles are formed with the maximum wrinkle amplitude occurring at the center of the membrane; which is the location where wrinkles initiate. Moreover, the wavelength of the largest wrinkle decreases whereas the wrinkle magnitude increases as more tensile strain is applied. Figure 7 compares the numerical and experimental wrinkling profiles at the transverse mid-plane at the strains of 2%, 3%, and 4%. It is observed from this figure that the wrinkling pattern, amplitude, and wavelength obtained experimentally from the DIC system agree well with the FE simulation results. The discrepancy seen next to the free edges of the membrane is due to rigid body rotations resulting from gripping the $25\,\mu m$ thick membrane as well as from imperfections introduced at the membrane boundaries when specimens were cut. Figure 8 shows the full field out of plane displacement of the membrane obtained from FE analysis and experiments at different strains (1%, 2%, 3%, 4%). Excellent agreement between experiments and simulations is seen for the full field out of plane displacement.

Figure 9 shows the variation of the minor principal stress and out of plane displacement at a strain of 4% along the transverse mid-plane of the membrane. It is deduced from this figure that the out of plane displacement and minor principal stress share the same fluctuating trend.

This observation will be used to develop the optimally designed geometric modifications (i.e., holes), which can effectively eliminate wrinkling.

Table 1: Effect of number of elements on the buckling strain and wrinkling amplitude.

Number of Elements	1250	2500	5000	7500	10000
Lowest eigenvalue	0.521	0.477	0.457	0.453	0.450
Wrinkling amplitude at a strain of 4% (mm)	0.0867	.08936	0.0974	0.0973	0.0971

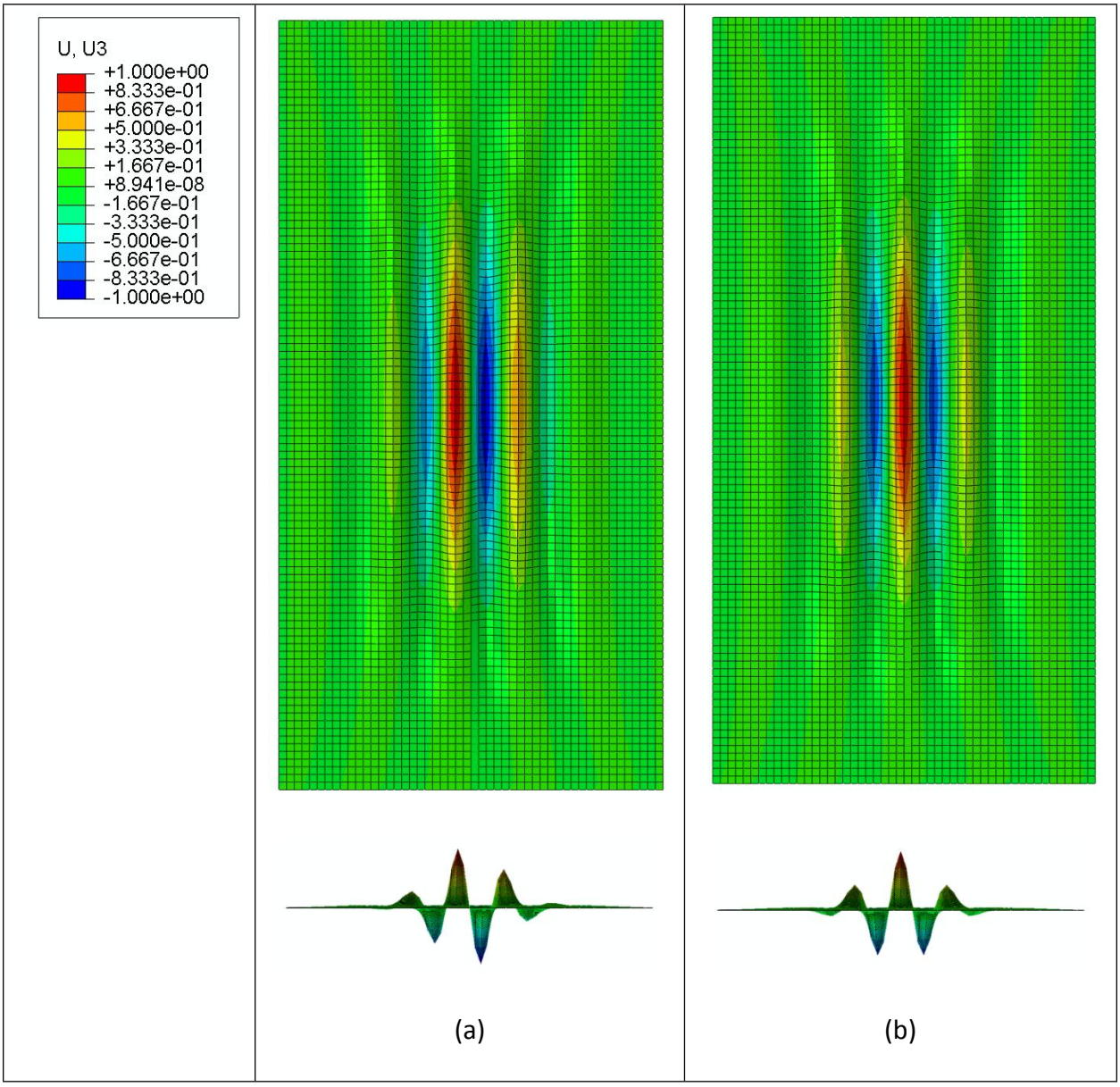

Figure 5. First two buckling modes (a) First (antisymmetric) buckling mode (b) second (symmetric) buckling mode. Front and bottom views of the two modes are shown.

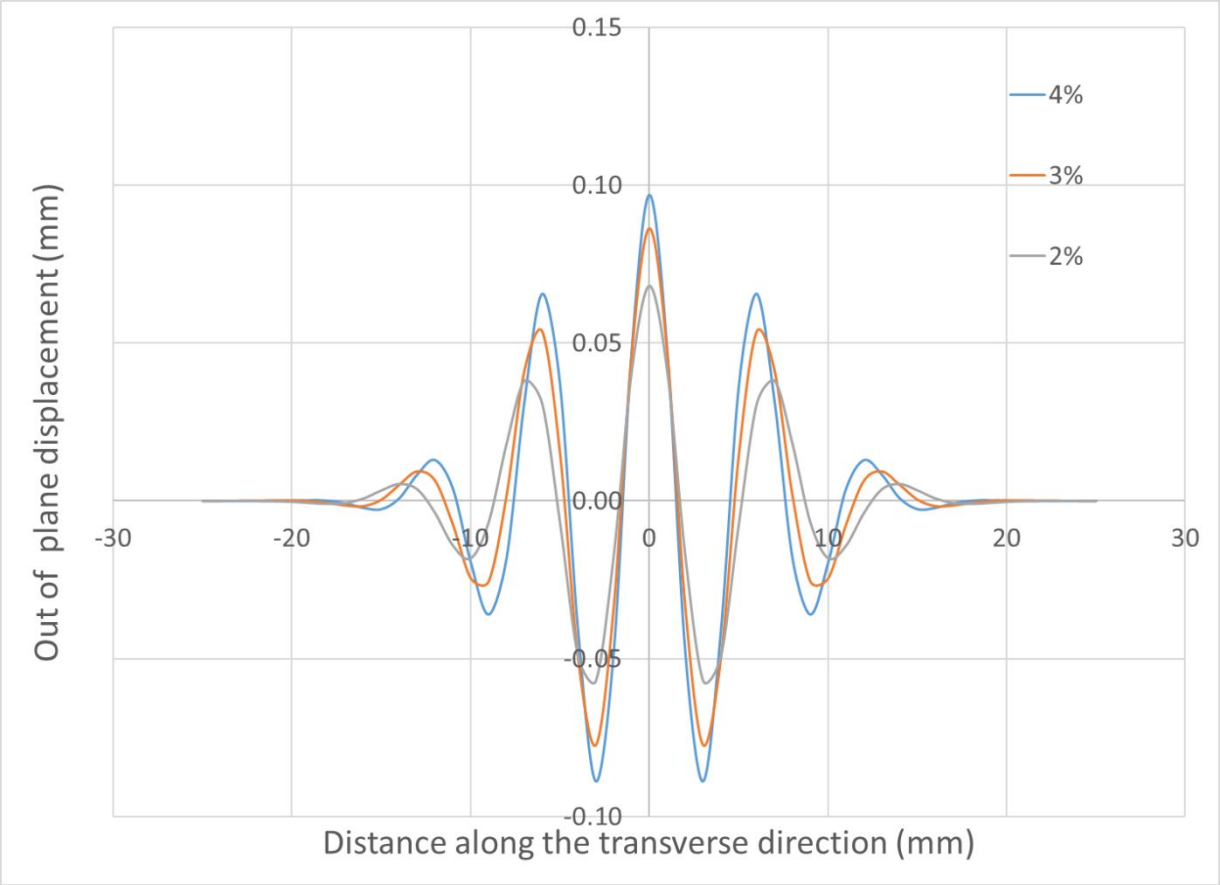

Figure 6. Wrinkling profile at the transverse mid-plane from FE simulations (Post buckling at stains of 2%, 3%, and 4%).

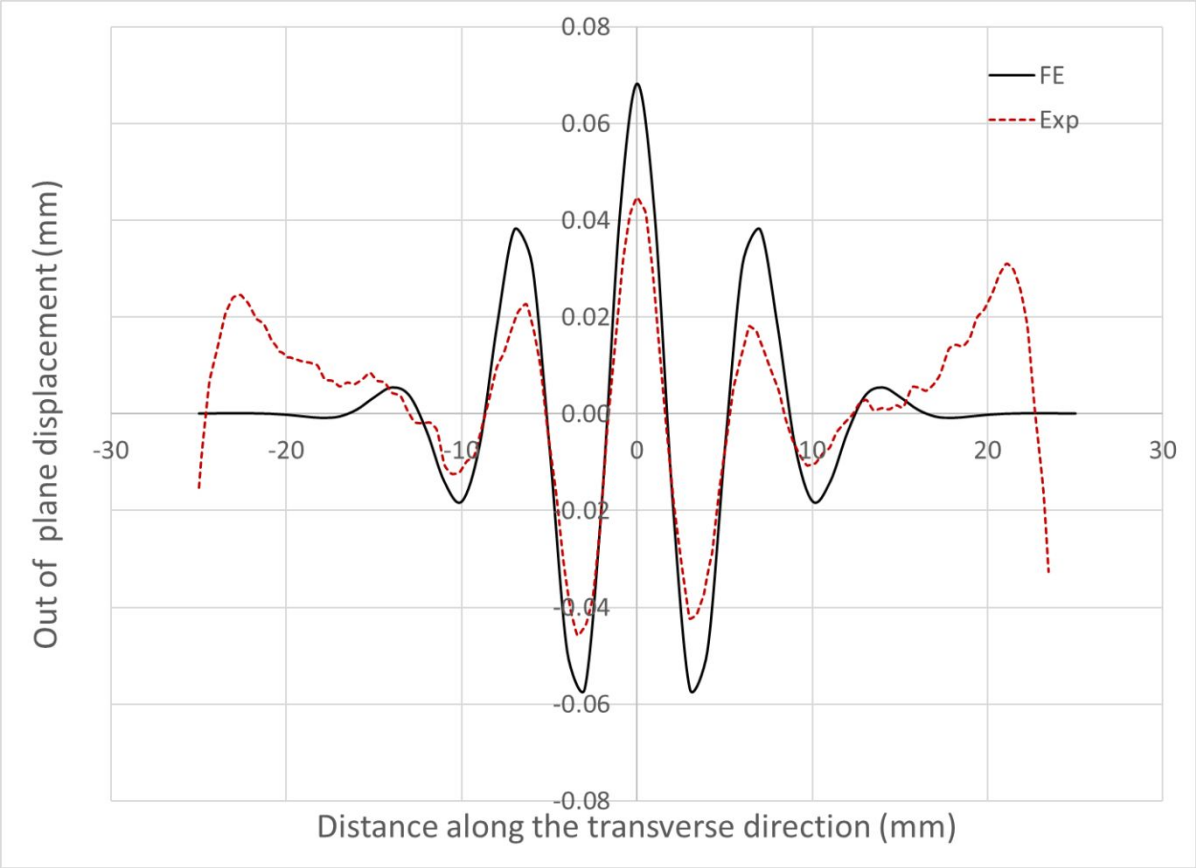

Figure 7 (a). Numerical and experimental wrinkling profiles at the transverse mid-plane at a strain of 2% (Post buckling).

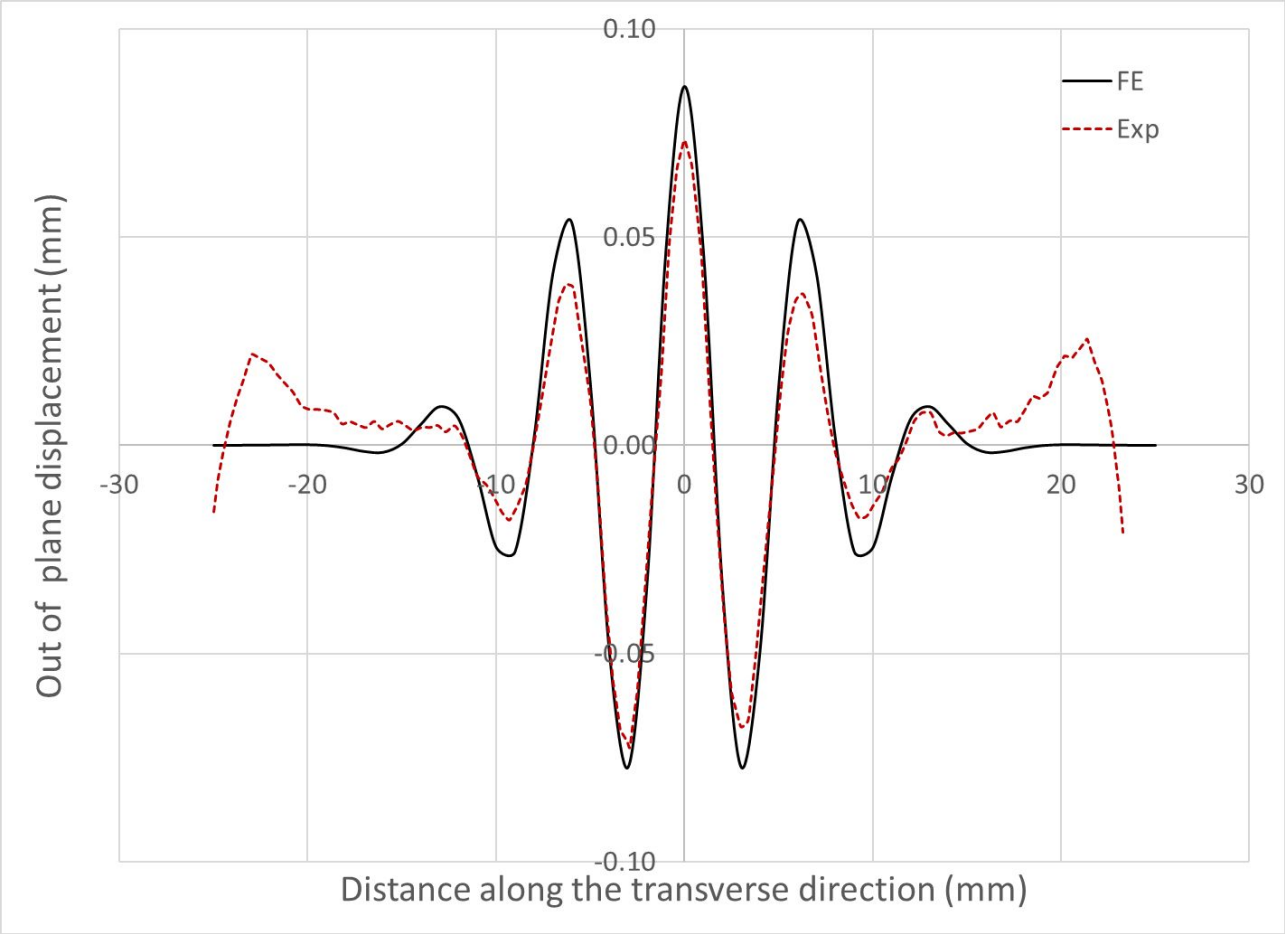

Figure 7 (b). Numerical and experimental wrinkling profiles at the transverse mid-plane at a strain of 3% (Post buckling).

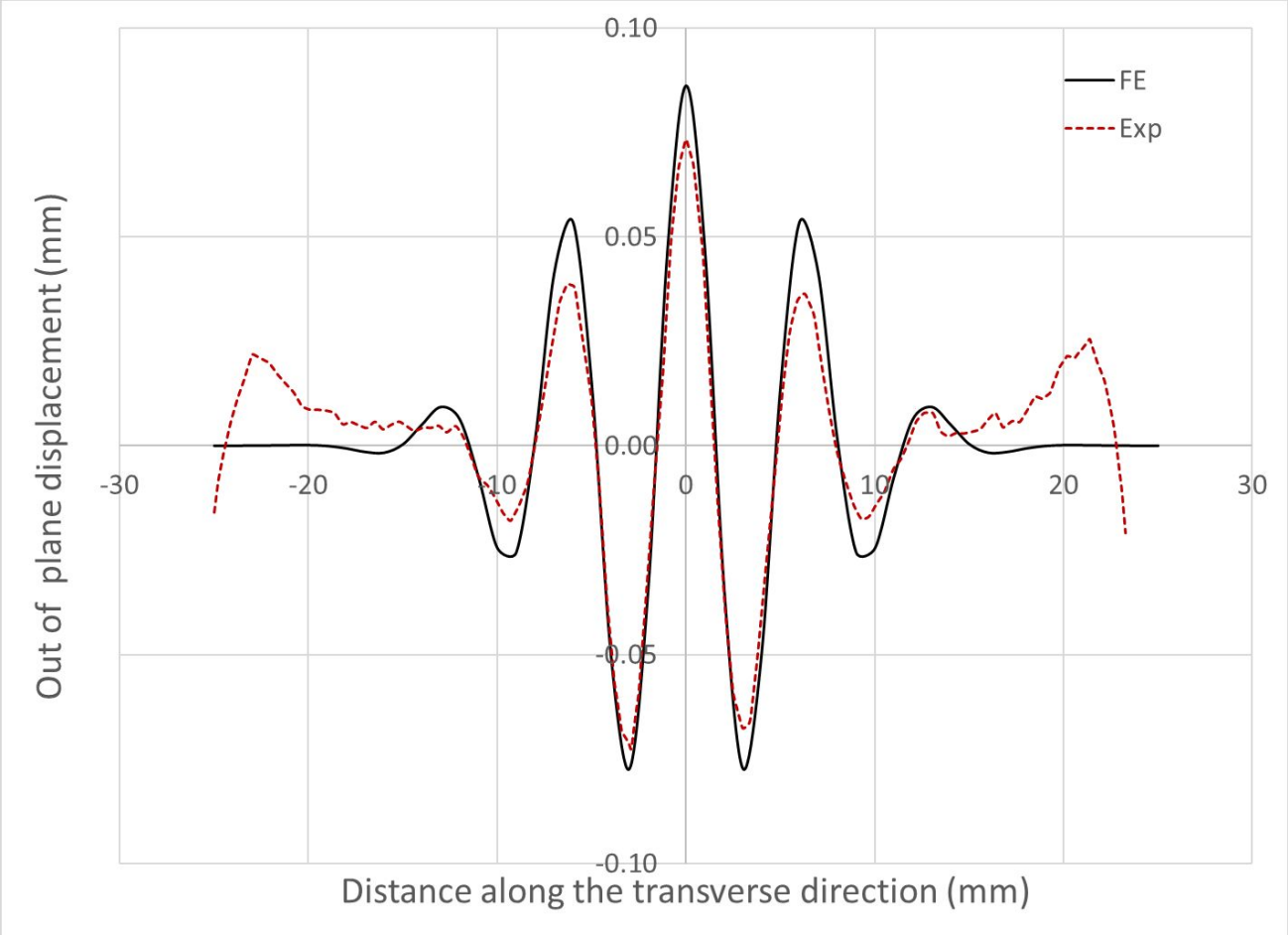

Figure 7 (c). Numerical and experimental wrinkling profiles at the transverse mid-plane at a strain of 4% (Post buckling).

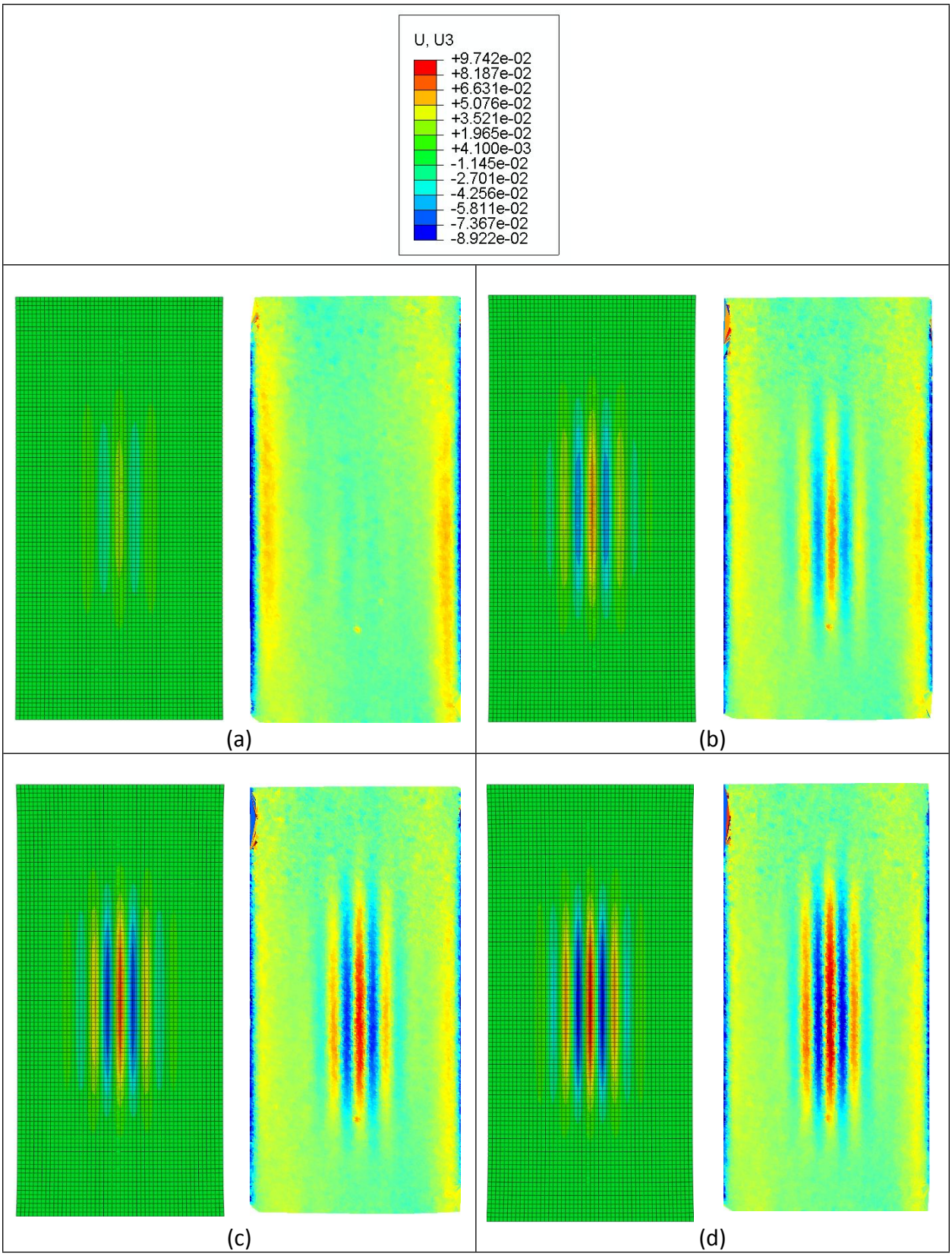

Figure 8. Full field out of plane displacement from FE simulations (left) and DIC system (right) at different strains (a) 1% (b) 2% (c) 3% (d) 4%. (Legend unit is mm)

Figure 9. Minor principal stress and wrinkle profile (post buckling) along the transverse mid-plane of the membrane.

3.2 Optimal membrane design for wrinkling suppression

It is concluded form Figure 9 that the wave like pattern of the minor principle stress leads to the formation of wrinkles. If the stress field is redistributed to eliminate the minor principal stress fluctuation in the deformed membrane, wrinkles will disappear. In this work, symmetric holes are introduced in the membrane to redistribute the stress field and suppress wrinkling in the deformed membrane. Figure 1 (b) shows a schematic for the membrane with symmetric circular holes. The location and size of the holes are two key factors that will alter the stress state to eliminate the minor principle stress fluctuation.

The Non Linear Programming by Quadratic Largrangian (NLPQL) technique is used to determine the location and size of the circular holes that lead to wrinkling suppression. In this method, a quadratic approximation is built to obtain a local optimum design. The process is repeated to find an improved design until it converges to a final optimum design. The objective is to minimize the summation of the absolute value of the post buckling out of plane displacement (U_3) in the whole membrane. A compressive stress index in the minor principal direction without the need of post buckling analysis can also be used as the objective function to suppress wrinkling. Both approaches lead to the same result as compressive stresses drive the wrinkling phenomena while the post buckling analysis measures the occurrence of the phenomena. However, if wrinkling cannot be completely eliminated or the wrinkling behavior has to be tailored for specific applications (i.e.: energy harvesting applications), the post buckling analysis is needed as the wrinkle amplitude, pattern, wavelength are obtained from post buckling analysis. The summation of the absolute value of the out of plane displacement is chosen here as an objective function to capture wrinkles of small amplitude that might occur in the modified

membrane; especially in the region around the designed holes. The diameter of the hole (d) and the distance between the hole center and the center line of the membrane (l_1) shown in Figure 1 (b) are defined as the design variables. The boundaries for the input variables were set as constraints in the algorithm. The optimization problem is formulated as follows:

Minimize $\{\boldsymbol{f_1(x)}\}$

where: $\boldsymbol{f_1(x)} = \sum|\boldsymbol{U_3}|$

subjected to:

$$\boldsymbol{0.3 < d < 5.0\ mm}$$

$$\boldsymbol{30 < l_1 < 48\ mm}$$

The FE model and the NLPQL algorithm are run in a loop using the Simulia Isight system integration tool [31]. The FE computation parameters (e.g., boundary conditions and loads) used with the geometrically optimized membrane are identical to those used with its parent membrane (i.e., without holes). Isight drives the design variables into Abaqus for execution and extracts the output variables for design optimization using the NLPQL algorithm that generates new values for the input variables. Figure 10 shows a flow chart of the optimization procedure. The results of the final optimum design are $d = 2\ mm$, $l_1 = 39\ mm$, and $\sum|U_3| = 0.013\ mm$.

The first two buckling mode shapes for the optimal design obtained from the FE simulations are shown in Figure 11. The eigenvalues associated with the two buckling modes are $\lambda_1 = 0.135$ and $\lambda_2 = 0.171$. It is noticed that the membrane buckles in the region around the hole; not in the middle of the membrane. The first buckling mode is introduced into the model as geometric imperfection for post buckling analysis. Figure 12 shows the full field out of plane displacement contour plot of the membrane obtained from FE analysis and experiments at

different strains (1%, 2%, 3%, 4%). It is seen from this figure that a wrinkle free flat surface exists in the middle of the membrane. Negligible noise (~$10^{-3}mm$) appears in the experimental results shown in Figure 12. Noise spreads across the specimen but increases in level at the membrane boundaries. Noise typically appears when DIC is used to measure small values. This particularly applies to Figure 12 as the out of plane displacement measured is zero. The experimental plots in Figure 12 are slightly smaller than their computational counterparts as the field of view of the cameras used to capture the images excluded a couple of millimeters near the grips. With respect to principal stresses in the case with optimally designed holes, only one small wrinkle appears in the vicinity of the hole. Figure 13 compares the minor principal stress along the transverse mid-plane for the optimal design against the non-modified membrane. On contrary to the fluctuating compressive minor stresses that occur in the non-modified membrane, the minor principal stress is non-fluctuating and exhibits a lower amplitude for the optimal design. As a result, wrinkles are fully suppressed in the middle of the membrane as shown in Figure 14.

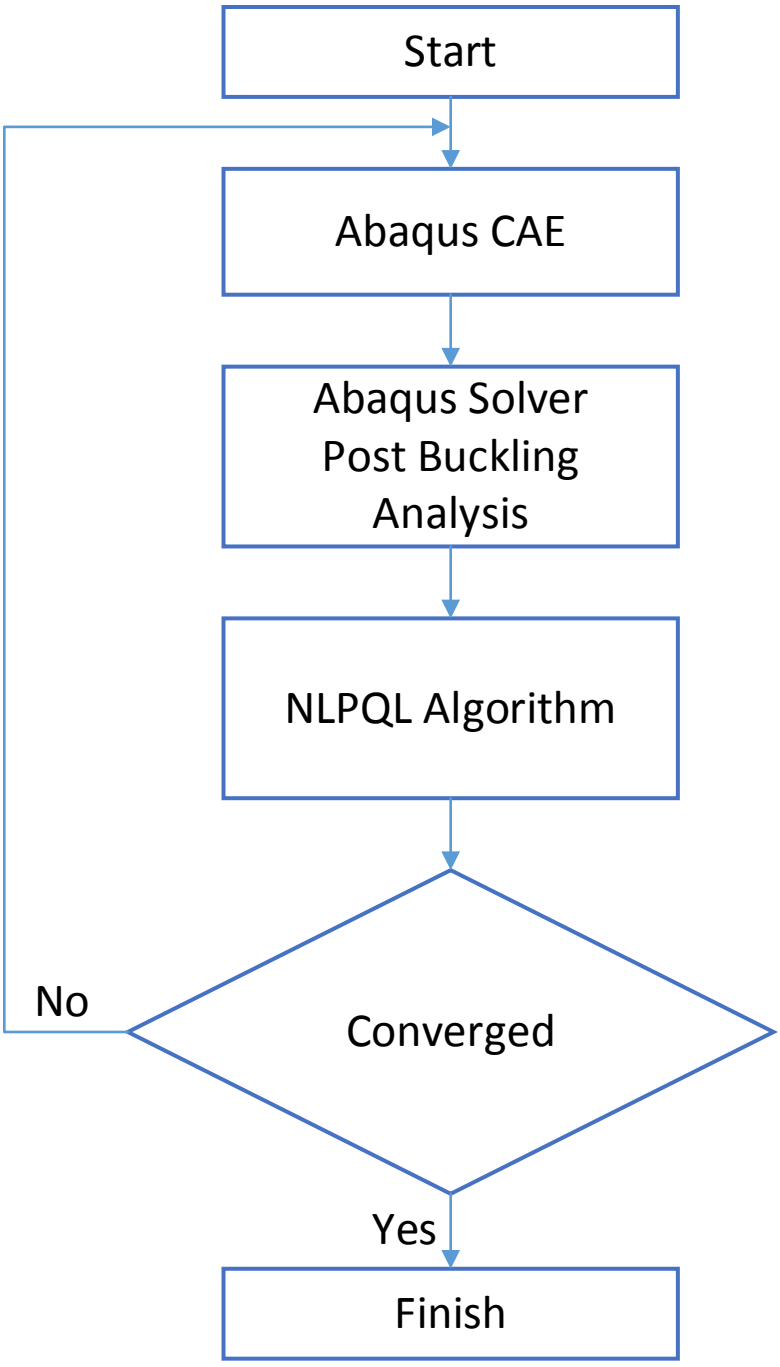

Figure 10. Flow chart of optimization procedure.

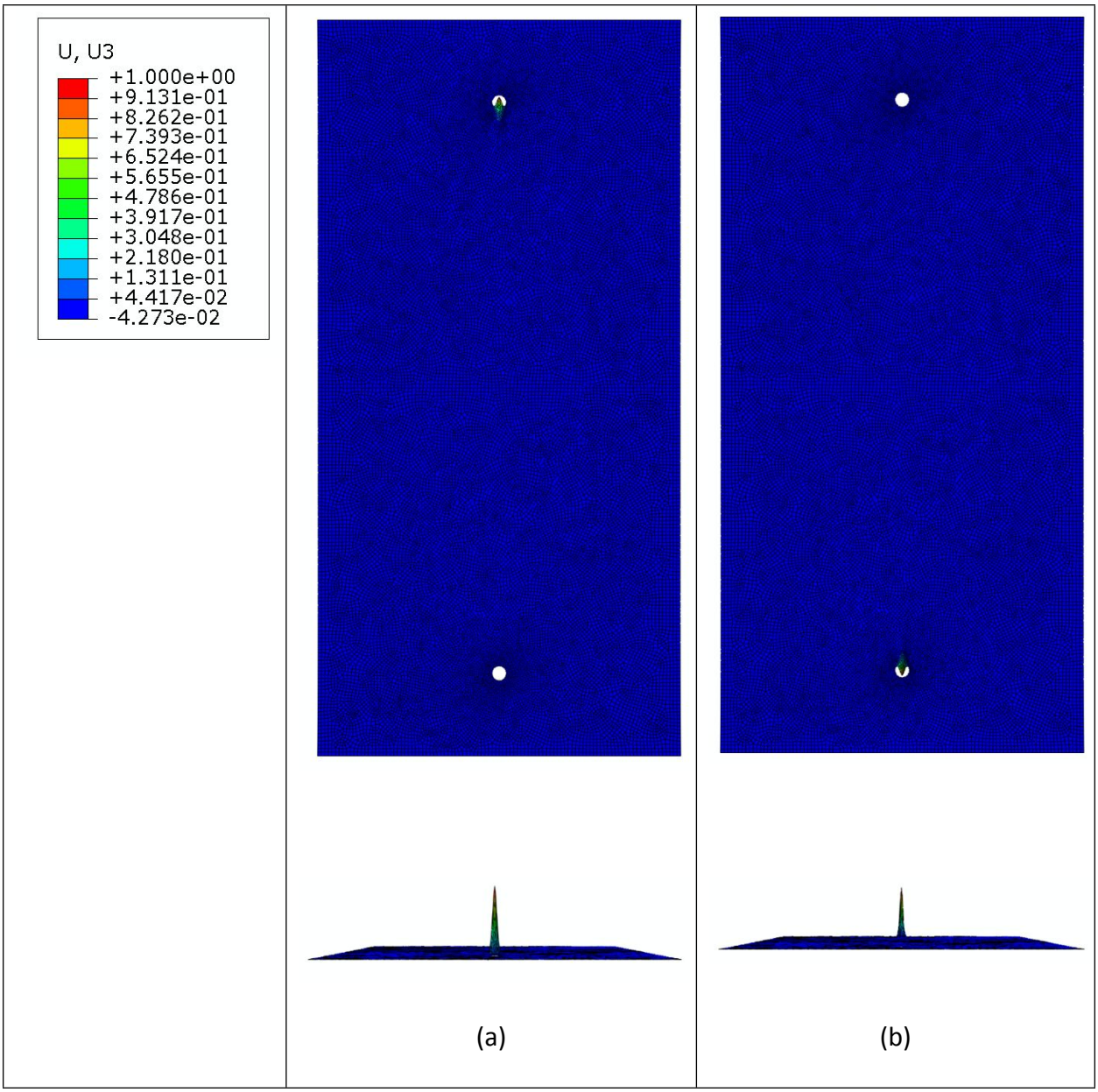

Figure 11. First two buckling modes (a) First buckling mode (b) Second buckling mode.

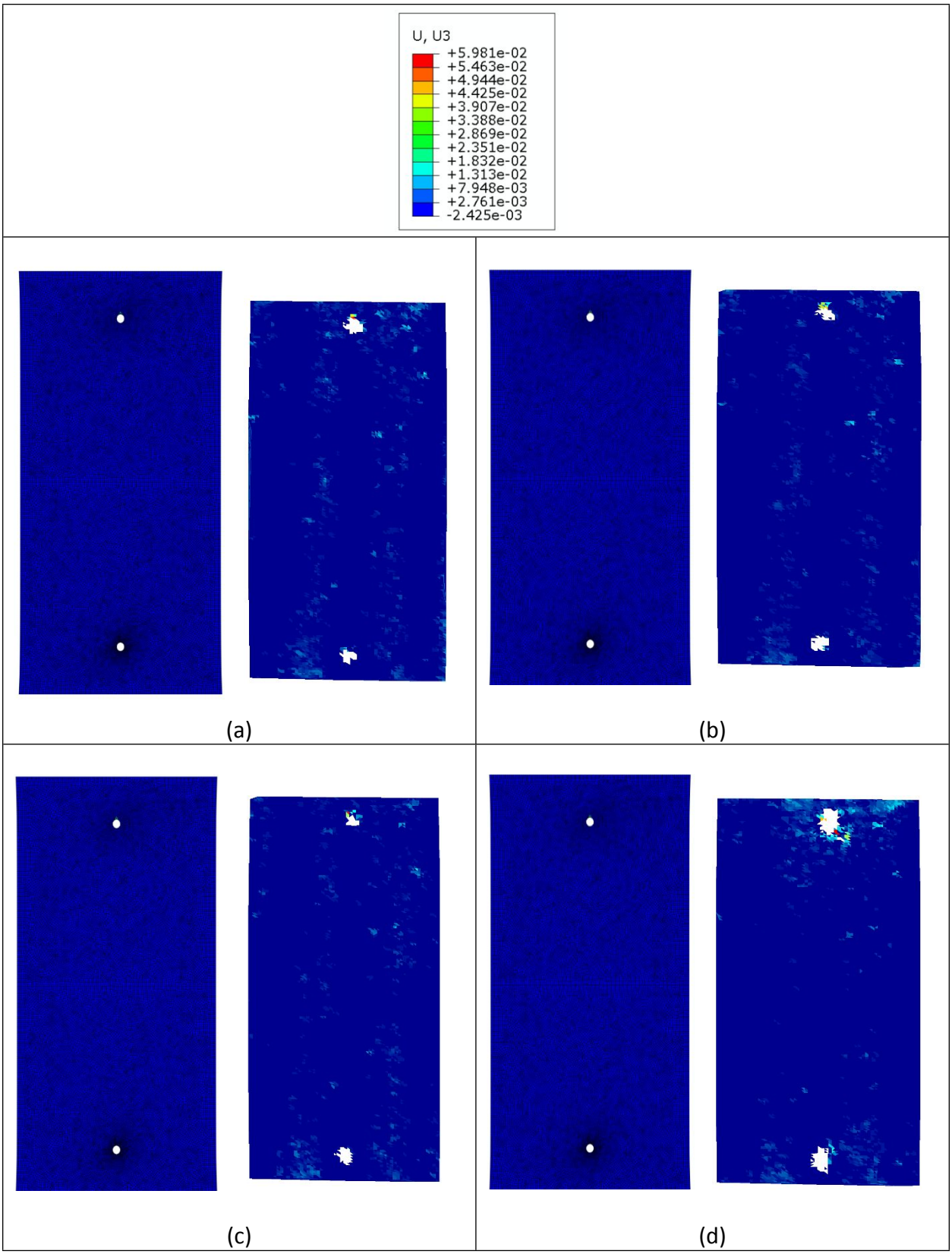

Figure 12. Full field out of plane displacement for the optimal design from FE simulations (left) and DIC system (right) at different strains (a) 1% (b) 2% (c) 3% (d) 4%. (Legend unit is mm)

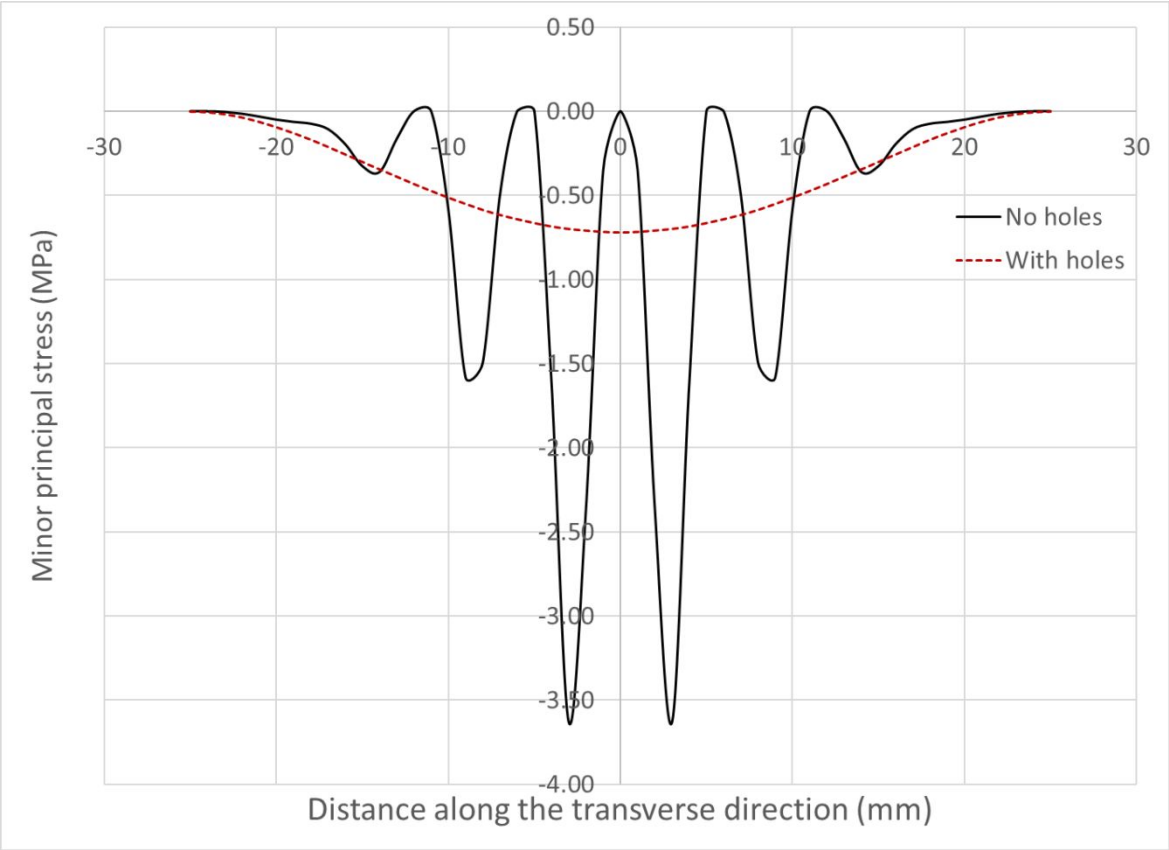

Figure 13. Minor principal stress (post buckling) along the transverse mid-plane of the membrane (membrane without holes vs optimal design).

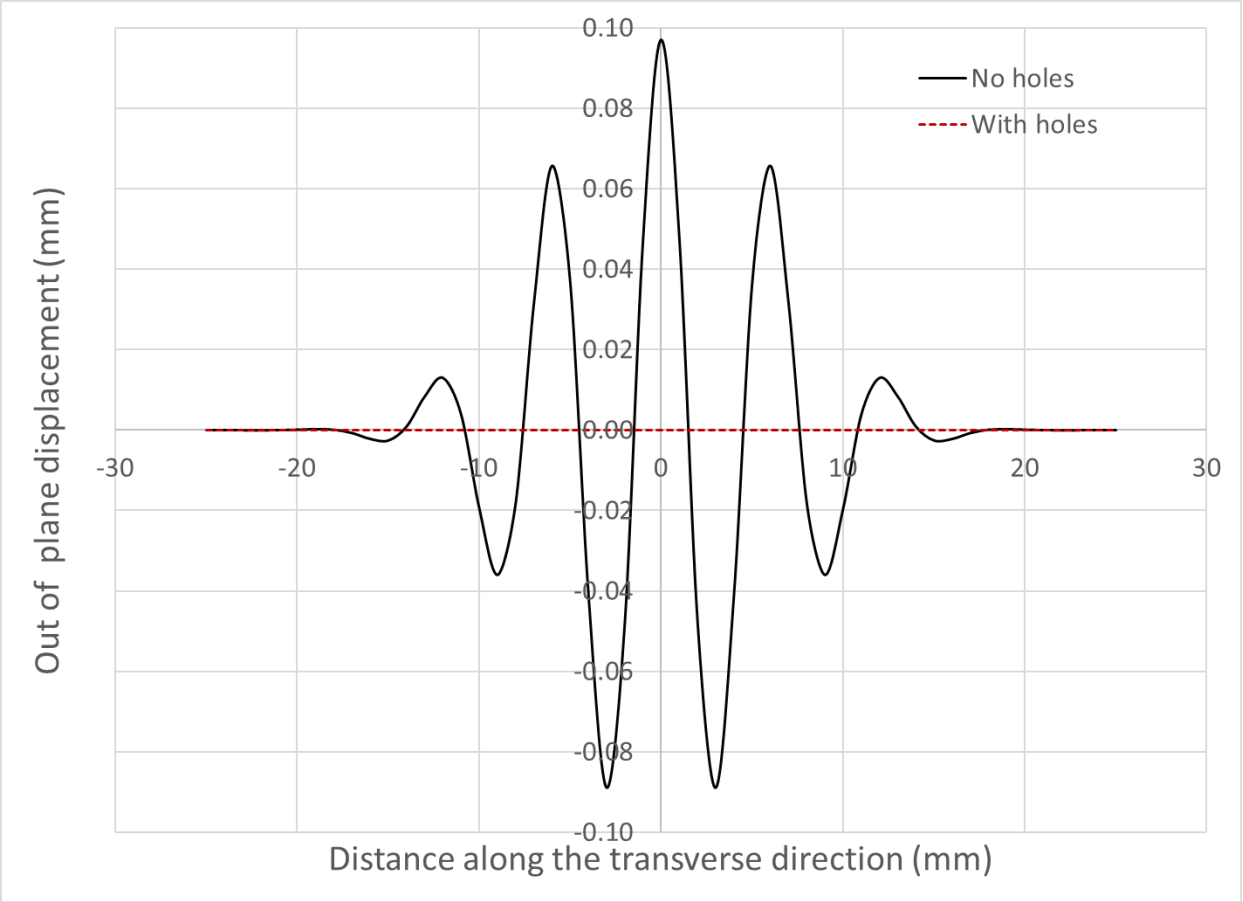

Figure 14. Wrinkling profiles (post buckling) obtained from FE at the transverse mid-plane at a strain of 4%

4. Conclusions

In this work, a new approach for wrinkling suppression in thin membranes is proposed and validated. The results obtained provide instrumental information that aids in wrinkle suppression of thin membranes subjected to elastic uniaxial stretching. The following conclusions were established from this investigation:

1- The wrinkling pattern, amplitude, and wavelength obtained from the developed FE model for the uniaxial stretching of the 25 μm thick membrane match the experimental results obtained from the full field DIC.

2- The introduction of symmetric circular holes in the membrane redistributes the stress field. The diameter and location of the holes for the optimal design is determined based on the NLPQL optimization algorithm with the goal of minimizing the summation of the absolute value of the out of plane displacement.

3- The fluctuating behavior of the minor principal stress along the transverse mid-plane is not present anymore in the optimal design. As a result, wrinkles are fully suppressed in the middle of the membrane. The full field DIC results show that zero out of plane displacement is observed in the middle of the membrane.

4- For the optimal design membrane, buckling occurs in the region around the circular hole. A single wrinkle that has low amplitude is developed in the post buckling analysis. This wrinkle was also observed in experiments using the full field DIC.

5- The approach used in this work is general and can be extended to materials that exhibit higher elastic strains for different applications such as flexible electronics and aerospace structures.

Acknowledgement

None

Funding

This work was supported by the American University of Sharjah under grant number EFRG18 MSE-CEN-26, FRG19-M-E78, FRG21-M-91.

Data Availability

The raw/processed data required to reproduce these findings cannot be shared at this time as the data also forms part of an ongoing study.

References

1. Mamleyev ER, Heissler S, Nefedov A, et al. Laser-induced hierarchical carbon patterns on polyimide substrates for flexible urea sensors. *npj Flexible Electronics*. 2019; 3: 2.
2. Romero FJ, Rivadeneyra A, Salinas-Castillo A, et al. Design, fabrication and characterization of capacitive humidity sensors based on emerging flexible technologies. *Sensors and Actuators B: Chemical*. 2019; 287: 459-67.
3. Zhang X, Grajal J, Vazquez-Roy JL, et al. Two-dimensional MoS2-enabled flexible rectenna for Wi-Fi-band wireless energy harvesting. *Nature*. 2019; 566: 368-72.
4. Overview Of Gossamer Structures. *Gossamer Spacecraft: Membrane And Inflatable Structures Technology For Space Applications*. American Institute of Aeronautics and Astronautics, 2001, p. 1-33.
5. Cunningham K, Fabisinski, L., Johnson, L., Justice, S. Lightweight Inflatable Solar Array: Providing a Flexible, Efficient Solution to Space Power Systems for Small Spacecraft. 2014.
6. McMahan T. Inflatable Solar Array Technology Packs Incredible Power In Small Package. 2014.
7. Wagner H. Flat sheet metal girder with very thin metal web. *Zeitschrift f_ur Flugtechnik und Motorluftschiffahrt*. 1929; 20: 200-314.
8. Stein M. Analysis of partly wrinkled membranes. *NASA TN, 1961*. 1961.

9. Ding H and Yang B. The modeling and numerical analysis of wrinkled membranes. *International Journal for Numerical Methods in Engineering*. 2003; 58: 1785-801.
10. Coman CD. On the applicability of tension field theory to a wrinkling instability problem. *Acta Mechanica*. 2007; 190: 57-72.
11. Iwasa T. Wrinkle-Reduction Law for Rectangular Membranes Under a Shear Load. *AIAA Journal*. 2018; 56: 2870-6.
12. Iwasa T. Experimental verification on wrinkling behavior given by wrinkling analysis using the tension field theory. *International Journal of Solids and Structures*. 2018; 136-137: 1-12.
13. Tomita Y and Shindo A. Onset and growth of wrinkles in thin square plates subjected to diagonal tension. *International Journal of Mechanical Sciences*. 1988; 30: 921-31.
14. Nayyar V, Ravi-Chandar K and Huang R. Stretch-induced stress patterns and wrinkles in hyperelastic thin sheets. *International Journal of Solids and Structures*. 2011; 48: 3471-83.
15. Lecieux Y and Bouzidi R. Experimental analysis on membrane wrinkling under biaxial load – Comparison with bifurcation analysis. *International Journal of Solids and Structures*. 2010; 47: 2459-75.
16. Wang T, Fu C, Xu F, Huo Y and Potier-Ferry M. On the wrinkling and restabilization of highly stretched sheets. *International Journal of Engineering Science*. 2019; 136: 1-16.
17. Deng X, Xu Y and Clarke C. Wrinkling modelling of space membranes subject to solar radiation pressure. *Composites Part B: Engineering*. 2019; 157: 266-75.
18. Delapierre M, Chakraborty D, Sader JE and Pellegrino S. Wrinkling of transversely loaded spinning membranes. *International Journal of Solids and Structures*. 2018; 139-140: 163-73.
19. Huang Q, Kuang Z, Hu H and Potier-Ferry M. Multiscale analysis of membrane instability by using the Arlequin method. *International Journal of Solids and Structures*. 2019; 162: 60-75.
20. Zheng L. Wrinkling of dielectric elastomer membranes California Institute of Technology, 2009.
21. Li M, Niu Y, Wu H, Zhang X, Luo Y and Kang Z. Wrinkling and wrinkling-suppression in graphene membranes with frozen zone. *Thin Solid Films*. 2017; 638: 345-53.
22. Luo Y, Xing J, Niu Y, Li M and Kang Z. Wrinkle-free design of thin membrane structures using stress-based topology optimization. *Journal of the Mechanics and Physics of Solids*. 2017; 102: 277-93.
23. Wang T, Yang Y, Fu C, Liu F, Wang K and Xu F. Wrinkling and smoothing of a soft shell. *Journal of the Mechanics and Physics of Solids*. 2020; 134: 103738.
24. Wang T, Yang Y, Fu C and Xu F. Competition between Mullins and curvature effects in the wrinkling of stretched soft shells. *International Journal of Solids and Structures*. 2022; 241: 111473.
25. Alberini R, Spagnoli A and Terzano M. Numerical modelling of wrinkled hyperelastic membranes with topologically complex internal boundary conditions. *International Journal of Mechanical Sciences*. 2021; 212: 106816.
26. Barsotti R, Ligarò SS and Royer-Carfagni GF. The web bridge. *International Journal of Solids and Structures*. 2001; 38: 8831-50.
27. Li M, Li Y, Zhang C, et al. Stiffness modulation-driven wrinkle-free membrane. *Applications in Engineering Science*. 2022; 9: 100087.

28. Bertoldi K, Reis PM, Willshaw S and Mullin T. Negative Poisson's Ratio Behavior Induced by an Elastic Instability. *Advanced Materials*. 2010; 22: 361-6.
29. Yan D, Zhang K, Peng F and Hu G. Tailoring the wrinkle pattern of a microstructured membrane. *Applied Physics Letters*. 2014; 105: 071905.
30. Dupont Kapton Polyimide Film General Specifications. *Bulletin GS-96-7*.
31. Abaqus/Standard Users Manual Dassault Systems Simulia Corp, Providence, RI, USA2017.
32. Carvalho RVd. Wrinkling of thin sheets under tension. Instituto Superior Técnico, 2015.